



# The Apparently Unreactive Substrate Facilitates the Electron Transfer for Dioxygen Activation in Rieske Dioxygenases

Katja-Sophia Csizi,<sup>[a, b]</sup> Lina Eckert,<sup>[b]</sup> Christoph Brunken,<sup>[a, b]</sup> Thomas B. Hofstetter,<sup>\*[a]</sup> and Markus Reiher<sup>\*[b]</sup>

**Abstract:** Rieske dioxygenases belong to the non-heme iron family of oxygenases and catalyze important *cis*-dihydroxylation as well as *O*-/*N*-dealkylation and oxidative cyclization reactions for a wide range of substrates. The lack of substrate coordination at the non-heme ferrous iron center, however, makes it particularly challenging to delineate the role of the substrate for productive O<sub>2</sub> activation. Here, we studied the role of the substrate in the key elementary reaction leading to O<sub>2</sub> activation from a theoretical perspective by systematically considering (i) the 6-coordinate to 5-coordinate conversion of the non-heme Fe<sup>II</sup> upon abstraction of a water ligand, (ii) binding of O<sub>2</sub>, and (iii) transfer of an electron from the Rieske cluster. We systematically evaluated the spin-state-dependent reaction energies and structural effects at the active site for all combinations of the three elementary processes in the

presence and absence of substrate using naphthalene dioxygenase as a prototypical Rieske dioxygenase. We find that reaction energies for the generation of a coordination vacancy at the non-heme Fe<sup>II</sup> center through thermoneutral H<sub>2</sub>O reorientation and exothermic O<sub>2</sub> binding prior to Rieske cluster oxidation are largely insensitive to the presence of naphthalene and do not lead to formation of any of the known reactive Fe-oxygen species. By contrast, the role of the substrate becomes evident after Rieske cluster oxidation and exclusively for the 6-coordinate non-heme Fe<sup>II</sup> sites in that the additional electron is found at the substrate instead of at the iron and oxygen atoms. Our results imply an allosteric control of the substrate on Rieske dioxygenase reactivity to happen prior to changes at the non-heme Fe<sup>II</sup> in agreement with a strategy that avoids unproductive O<sub>2</sub> activation.

## Introduction


Dioxygen activation by mononuclear non-heme iron oxygenases is a central element in metabolic reactions in biology.<sup>[1–14]</sup> The range of biological functions associated with non-heme oxygenases include, for instance, natural product biosynthesis in  $\alpha$ -ketoglutarate-dependent oxygenases,<sup>[15,16]</sup> repair of methyl lesions in DNA by oxoglutarate-dependent oxygenases,<sup>[17]</sup> and biodegradation of recalcitrant aromatic pollutants by Rieske dioxygenases and catechol dioxygenases.<sup>[11,12,18–20]</sup> Mononuclear non-heme iron enzymes all share the structural motif in which


the catalytically active iron species is anchored in the 2-His-1-Carboxylate facial triad with up to three iron coordination sites being available for binding exogenous ligands such as solvents, the substrate and the co-substrate dioxygen.<sup>[21–27]</sup> Mechanistic investigations on the versatile chemistry of this class of enzymes revealed how substrate and cosubstrate interact with non-heme iron to generate high-valent iron species.<sup>[11,19,28–32]</sup> Despite these works, the path to dioxygen activation of Rieske dioxygenases (RDOs) remains somewhat elusive.<sup>[32,33]</sup> RDOs are the primary oxygenases responsible for the hydroxylation of aromatic hydrocarbons,<sup>[19,34–37]</sup> hence making them particularly relevant for bacterial metabolism of xenobiotic compounds. In contrast to other mononuclear non-heme iron oxygenases, however, substrates of RDOs are held in substrate pockets in the proximity of the active site but lack any bonding to the non-heme iron center.<sup>[22,38,39]</sup> Nevertheless, coordination and activation of O<sub>2</sub> at the non-heme iron center only proceeds in the presence of the substrate suggesting some allosteric control of substrate binding. Assigning a sequence of molecular events that lead to O<sub>2</sub> coordination and activation for substrate hydroxylation in RDOs is therefore particularly challenging.<sup>[9,20–22,24,30,40–42]</sup>


Reduction equivalents for O<sub>2</sub> activation in RDOs are provided by long-range electron transfer from an NADH reductase<sup>[12,37,43]</sup> through a Rieske [2Fe-2S] ferredoxin to the Rieske cluster of the oxygenase component in the  $\alpha_3\beta_3$  hexameric enzyme.<sup>[19,24,44]</sup> In their resting state, RDOs exhibit a

[a] K.-S. Csizi, Dr. C. Brunken, Priv.-Doz. Dr. T. B. Hofstetter  
Eawag, Swiss Federal Institute of Aquatic Science and Technology,  
Überlandstrasse 133, 8600 Dübendorf, Switzerland  
E-mail: thomas.hofstetter@eawag.ch

[b] K.-S. Csizi, L. Eckert, Dr. C. Brunken, Prof. Dr. M. Reiher  
ETH Zürich, Laboratory for Physical Chemistry, Vladimir-Prelog-Weg 2, 8093  
Zürich, Switzerland  
E-mail: markus.reiher@phys.chem.ethz.ch

 Supporting information for this article is available on the WWW under  
<https://doi.org/10.1002/chem.202103937>

 Part of the Chemistry Europe joint Special Collection on Quantum Bioinorganic Chemistry.

 © 2022 The Authors. Chemistry - A European Journal published by Wiley-VCH GmbH. This is an open access article under the terms of the Creative Commons Attribution Non-Commercial NoDerivs License, which permits use and distribution in any medium, provided the original work is properly cited, the use is non-commercial and no modifications or adaptations are made.

reduced non-heme Fe center which is linked through an aspartate residue to the reduced Rieske cluster (i.e., its  $\text{Fe}^{\text{II}}\text{-Fe}^{\text{III}}$  form) of an adjacent  $\alpha$ -subunit of the oxygenase (Figure 1).<sup>[45–47]</sup>  $\text{O}_2$  activation and initial steps of substrate hydroxylation result from the interplay of three main processes: (i) changes of the coordination polyhedron of the non-heme iron species from 6-coordinate to 5-coordinate ('6C' to '5C') through the release of a water ligand to generate a coordination vacancy (Figure 1, I  $\rightarrow$  II), (ii)  $\text{O}_2$  binding at the non-heme  $\text{Fe}^{\text{II}}$  site, and (iii) electron transfer from the Rieske cluster to non-heme Fe (II  $\rightarrow$  III). None of the three processes appears to require an interaction of the active site species with the substrate, yet they only occur in the presence of the substrate.<sup>[5,48]</sup> Moreover, the substrate is typically located in an average distance of 4.5–5.0 Å to the non-heme Fe center, and hence, too far away to exert direct electronic effects on the active-site chemistry.

The two current mechanistic hypotheses for  $\text{O}_2$  activation and substrate hydroxylation by RDOs both reveal ambiguities regarding the sequence and mechanism of  $\text{O}_2$  binding and electron transfer from the Rieske cluster. The so-called native  $\text{O}_2$  reaction proceeds through a high-spin  $\text{Fe}^{\text{III}}$ -superoxo species<sup>[33]</sup> that attacks the substrate and leads to an  $\text{Fe}^{\text{III}}$ -OH substrate epoxide through formation of an  $\text{Fe}^{\text{III}}$ -peroxy-aryl radical. The reaction is driven by a proton-coupled electron transfer concomitant with Rieske cluster oxidation, followed by O–O

bond cleavage, and ultimately, dihydroxylation.<sup>[33]</sup> By contrast, the so-called peroxide shunt mechanism implies Rieske cluster oxidation prior to generation of a reactive  $\text{Fe}^{\text{III}}$ -hydroperoxy intermediate,<sup>[31,36,38]</sup> or alternatively, its rearrangement to an  $\text{HO-Fe}^{\text{IV}}=\text{O}$  species that enables substrate attack.<sup>[19,31,37,50–52]</sup> While these mechanistic conclusions were drawn from studies of various RDOs and substrates,<sup>[11,19,21,32,33,49,50,53,54]</sup> contributions of substrate interactions at the active site to  $\text{O}_2$  activation remain largely elusive. Naphthalene- and benzoate-dioxygenases, for example, do not exhibit specific interactions in the hydrophobic substrate binding pocket whereas nitrobenzene- and carbazole-dioxygenases bind the substrate through H-bonding with amino acid residues.<sup>[55,56]</sup> However, these interactions poorly affect any of the  $\text{O}_2$  activation processes introduced above. It is reported that spontaneous release of one water ligand is induced upon substrate binding to open up the six-fold coordination environment and create a coordinatively unsaturated site.<sup>[9,20–22,24,30,40–42]</sup> This reaction was hypothesized as a consequence of steric hindrance between substrate and water molecule.<sup>[11]</sup> Furthermore, the requirement of a reduced Rieske cluster implies that its redox state and the affinity of the mononuclear iron center for  $\text{O}_2$  coordination and substrate binding are coupled. ENDOR spectroscopy showed that the oxidation state of the Rieske cluster modulates the relative orientation of substrate and metal center by a distal

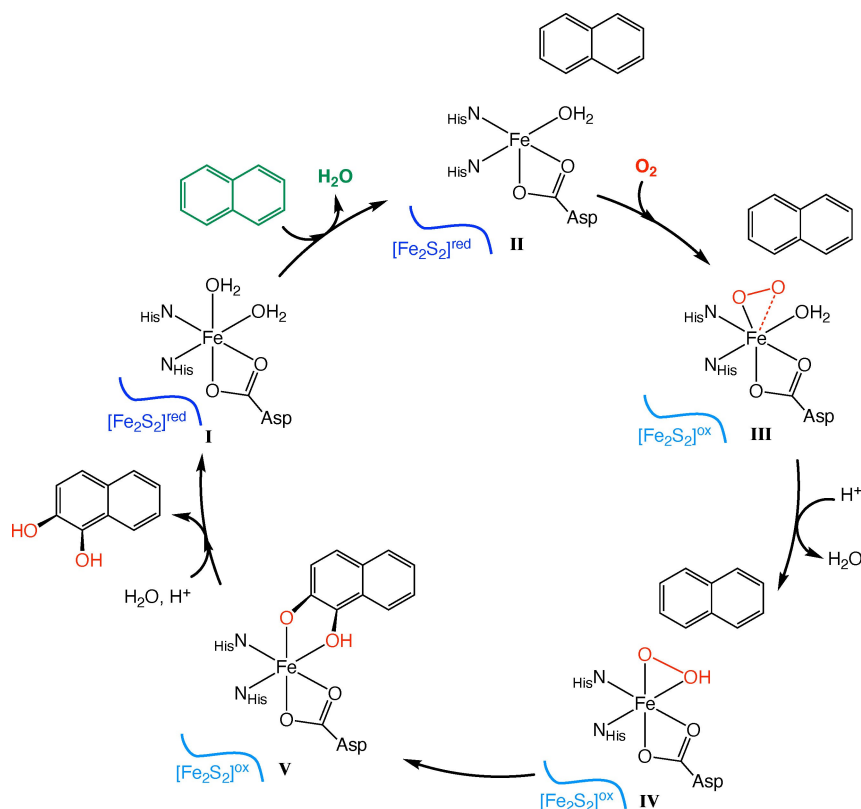


**Figure 1.** Catalytic cycle of naphthalene 1,2-dioxygenase and its native substrate, naphthalene, used as a model for oxygenations catalyzed by Rieske dioxygenases. The transition from  $[\text{Fe}_2\text{S}_2]^{\text{red}}$  to  $[\text{Fe}_2\text{S}_2]^{\text{ox}}$  in reaction II  $\rightarrow$  III denotes the electron transfer from the Rieske cluster to the non-heme Fe. Iron oxidation states are omitted for the sake of simplicity. Note that the Fe-peroxy species (IV) shown for NDO is one of several proposed reactive Fe– $\text{O}_2$  species of RDOs responsible for aromatic hydroxylation reactions (see text).<sup>[33,49]</sup>

shift of about 0.5 Å, coupled to conformational changes at one histidine ligand to open the site for dioxygen to enter.<sup>[11,21,32,36,41,45,48,51,57,58]</sup> These observations all imply a tight control of O<sub>2</sub> activation and reactivity<sup>[9,59]</sup> by the enzyme whereas the role of enzyme-substrate interactions on the sequence of these processes at the non-heme Fe of RDOs remains unclear. Our work aims at characterizing the role of the substrate in the elementary steps leading to O<sub>2</sub> activation in Rieske dioxygenases from a theoretical perspective. Our quantum chemical model approach allows us to dissect various structural effects on these processes. Based on tailored structural models, we present a systematic evaluation of all possible elementary reaction sequences of the non-heme coordination environment and active-site chemistry of RDOs. With naphthalene dioxygenase, NDO, as a prototypical RDO, we assess the contribution of its native substrate, naphthalene, onto the reaction energies of (i) the release of a H<sub>2</sub>O ligand, (ii) coordination of O<sub>2</sub> at the non-heme Fe<sup>II</sup>, and (iii) transfer of an electron by Rieske cluster oxidation. To this end, each of the reactions leading from species I to III in Figure 1 was evaluated in the absence and presence of the substrate. The chosen model is intentionally local and fully quantum mechanical to study the generic chemistry of substrate-modulated O<sub>2</sub> activation in RDOs. We account for a protein environment through the comparison of two structural models that represent the limiting cases of complete rigidity vs. absence of any structural constraints. To address the electron transfer from the proximate Rieske domain and changes of spin state during transition metal catalysis,<sup>[60]</sup> we follow a combined approach, in which we pre-sample the reaction space with Density Functional Theory (DFT) and apply coupled cluster reference calculations for critical steps. Finally, we qualitatively evaluate the underlying wave function with CASSCF calculations for selected steps where we expect a potential multiconfigurational character.

## Methodology

### Computational Methodology

DFT calculations were carried out with the TURBOMOLE suite of programs, version 7.2.0.<sup>[61]</sup> DFT structure optimizations applied the Perdew-Becke-Ernzerhof PBE<sup>[62]</sup> and corresponding hybrid PBE0<sup>[63,64]</sup> density functionals and a Ahlrichs def2-TZVP basis set.<sup>[65]</sup> The resolution-of-the-identity density-fitting technique was exploited for all PBE calculations.<sup>[66,67]</sup> For the Rieske cluster, in which two high-spin iron sites couple antiferromagnetically to yield an open-shell singlet state, a broken-symmetry DFT approach was applied by converging to the high spin solution and then flipping electrons at a local site. Grimme's D3 dispersion correction was invoked in all DFT calculations.<sup>[68,69]</sup> We applied the orbital perturbation protocol<sup>[70]</sup> for open-shell singlet structures to make sure that the lowest-energy was found in the Kohn-Sham DFT calculations as we observed that standard self-consistent-field convergence yielded local minima that are higher in energy in the space of the molecular orbital coefficients.

Coupled cluster single-point calculations in a def2-TZVP basis were carried out with ORCA 4.2.0<sup>[71,72]</sup> for PBE and PBE0 minimum structures on dioxygen coordination and electron transfer steps in the reaction network. The domain-based local-pair natural orbitals variant including perturbatively connected triple excitations, DLPNO-CCSD(T), was chosen.<sup>[73,74]</sup> The default NormalPNO convergence criteria were selected (see the Supporting Information for a comparison to tighter thresholds). We evaluated the multiconfigurational character of the wave function for selected complexes with Density Matrix Renormalization Group (DMRG) and CASSCF methods. CASSCF and DMRG calculations were carried out with OpenMolcas<sup>[75,76]</sup> and the QCMAQUIS DMRG program,<sup>[77,78]</sup> respectively, in combination with the automated active-space selection protocol<sup>[79–82]</sup> implemented in autoCAS.<sup>[83]</sup> Two-electron integrals were approximated by Cholesky decomposition.<sup>[84]</sup> The ANO-RCC-MB and ANO-RCC-VDZ basis sets were chosen for all atoms.<sup>[85]</sup>

We report electronic energy differences in kJ mol<sup>-1</sup> at zero Kelvin as an approximation to reaction enthalpies. This choice avoids the approximate description of translational and vibrational entropy contributions in the condensed phase. All charges and spin populations were obtained from Löwdin population analyses.<sup>[86]</sup> Bond orders were taken from Wiberg bond order analyses.<sup>[87]</sup> Structures were visualized with PYMOL 1.8.2.<sup>[88]</sup>

### Structural Models

The reactions studied are all sequences of elementary steps leading from I to III in Figure 1. They comprise (i) substrate binding, (ii) 6-to-5 coordination number conversion at the non-heme Fe site through release of a water molecule, (iii) electron transfer to the non-heme Fe site by Rieske cluster oxidation, and ultimately, (iv) coordination of dioxygen to the metal center. Since the substrate-driven activation of O<sub>2</sub> has been observed for all RDOs, we considered their shared structural motif, that is the mononuclear-non-heme active-site complex, a suitable minimal structural model. In this model, all residues in the first coordination sphere were included. For NDO, this comprised His<sub>208</sub>, His<sub>213</sub> and Asp<sub>362</sub>, which together form the well-known facial triad. Additionally, we incorporated the substrate naphthalene, two solvent-derived H<sub>2</sub>O ligands, and Asn<sub>201</sub>, which is hydrogen bonded to one H<sub>2</sub>O ligand. The resulting structure is shown in Figure 2 (left). We extracted this initial structure from the crystal structure of NDO with bound naphthalene (PDB-ID: 1O7G<sup>[38]</sup>). A model for the Rieske cluster (see Figure 2, right) was only required to obtain information on ionization energies and electron affinities and was considered separately. We dissected the electron transfer from the redox-active Rieske site to the non-heme Fe<sup>II</sup> site in two separate structural models: First, reduction of the non-heme iron active site was modeled by adding an electron to the active-site model, that is by increasing the number of electrons of this system. Second, oxidation of the Rieske cluster through ionization was evaluated. Only if the ionization energy of the Rieske cluster was smaller than the electron affinity of the non-

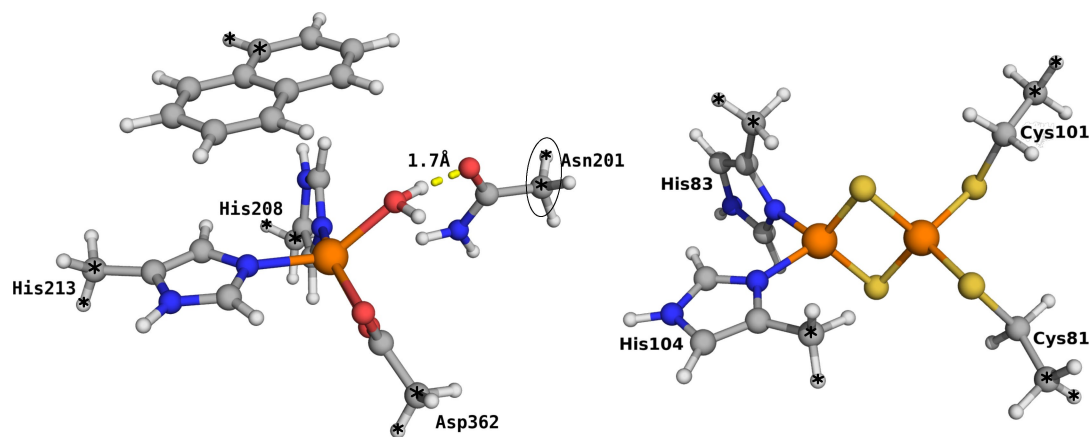


**Figure 2.** Models for the active site (left) and Rieske domain (right) of naphthalene 1,2-dioxygenase (NDO) extracted from the crystal structure with PDB-ID:1O7G.<sup>[38]</sup> All terminal bonds were saturated with hydrogen atoms prior to structure optimization. Atoms marked with an asterisk were kept frozen in the structure optimization of the constrained model. The atoms marked by an ellipse were subsequently frozen in the relaxed model. Color code: gray: carbon, red: oxygen, white: hydrogen, blue: nitrogen, yellow: sulfur, orange: iron.

heme Fe site, did we assume the electron transfer to occur spontaneously. By virtue of this approach, we can explicitly compare the electron affinity of each compound to a fixed ionization potential of the Rieske cluster and hence define a point at which an electron transfer step is thermodynamically favored (apart from the fact that a better estimate for the Rieske cluster ionization potential can be easily taken into account). Two structure model classes define the limiting cases of (i) a structurally constrained and of a (ii) fully relaxed system. The first class of models was obtained by freezing all terminal bonds in the aforementioned active-site model through Cartesian constraints according to the X-ray crystallography data (Figure 2). In the second class of models, all coordinates are fully relaxed apart from a single coordinate in the side chain that needed to be fixed to maintain structural integrity (atoms in Figure 2 marked by an ellipse). This fully relaxed model is designed to exhibit the generic reactivity of the active site where the steering structural constraints of the protein are switched off. It can be expected that the constrained model accounts for structural restraints of the protein backbone in a too restrictive manner, whereas the unconstrained model is too flexible. The true behavior is expected to lie in between these two limiting cases and structural effects can be captured from comparison of the fully relaxed and constrained model.

For both structure model classes, we generated the same reaction sequences that are spanned by all relevant elementary reaction steps. Evaluation of the corresponding reaction energies was then carried out twice, that is with and without the substrate naphthalene close to the active site. In total, this approach resulted in 24 intermediate structures for each class, as shown in Figure 3. For each structure, we considered various spin states. To probe for the effect of the specific choice of the exchange-correlation energy functional, we evaluated all spin states and reactions for two DFT functionals, PBE and PBE0. Energies and bond lengths refer to PBE-optimized structures unless stated otherwise. To probe for the effect of known limitations of contemporary DFT, we also provide *ab-initio* data

from coupled cluster calculations on a selected subset of elementary reactions for which, according to the DFT calculations, the substrate naphthalene may play a critical role for O<sub>2</sub> coordination and electron transfer. We specifically carried out CASSCF calculations on selected compounds for a qualitative characterization of the underlying wave function. We excerpt key results in our discussion and refer to the Supporting Information for the complete dataset including a spin state discussion and all optimized structures (see sections S3, S4, S9, and S10 in the Supporting Information).

Our overall approach is conceptualized in Figure 3, where we introduce the following short-hand notation: 1 refers to a 6-coordinate (6C) iron species. 2 is a 5C iron species with a water ligand bound to the Asn<sub>201</sub> residue, whereas 3 is a 5C iron species with the water ligand completely removed. A tilde (~) denotes the presence of the substrate naphthalene. Superscript *r* indicates a one-electron reduction, superscript **O2** refers to the presence of an O<sub>2</sub> molecule in the active site. In the following, we first evaluate the structural similarity between optimized structures of model structures and the corresponding experimental crystal structures, namely the substrate-free 6C site 1 (PDB-ID: 1NDO) and the substrate-bound 5C iron site  $\tilde{2}$  (PDB-ID: 1O7G). Second, we compare characteristic bond lengths between the non-heme Fe<sup>II</sup> center and the respective H<sub>2</sub>O ligands to available spectroscopic data for NDO.<sup>[38,89]</sup> Finally, we assess whether reaction energies for 6-to-5 coordination number conversion and substrate binding obtained with the constrained and fully relaxed model follow the same overall trends. Afterwards, we select one model for the evaluation of O<sub>2</sub> binding and electron transfer.

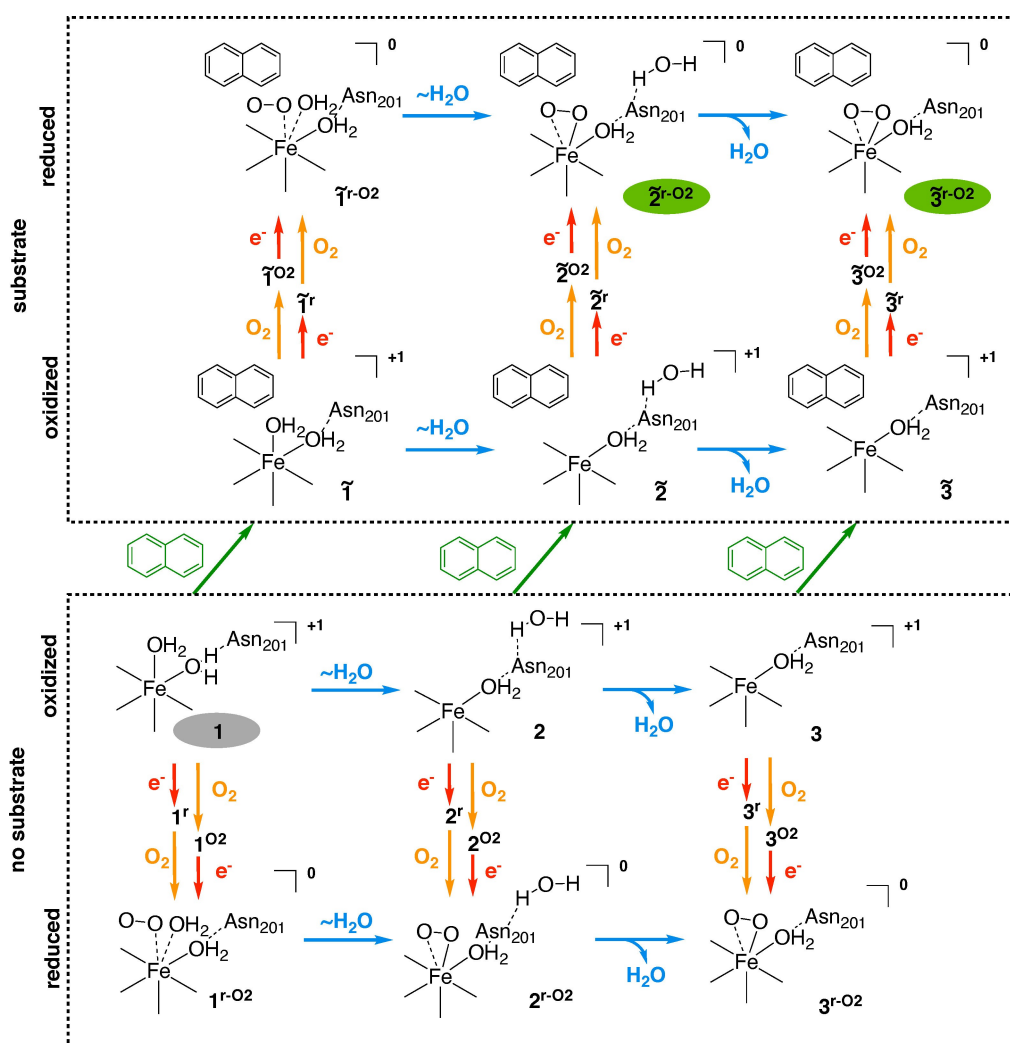


**Figure 3.** Schematic representation of elementary reactions for O<sub>2</sub> activation by NDO. Color code of reaction arrows: green: naphthalene binding; blue: water reorientation or abstraction, red: dioxygen addition; orange: one-electron reduction. Species that qualify for *cis*-dihydroxylation are circled in green spheres. The starting point of the network is circled in a gray sphere. The structures of possible intermediates that are formed depending on the sequence of dioxygen binding and reduction (in between orange and red arrows) are not explicitly shown for the sake of brevity. Note that we also consider water reorientation instead of water abstraction on the 6-to-5 coordination conversion pathway (denoted ~H<sub>2</sub>O). Oxidation states on iron are omitted for simplicity and are discussed in the text. The side-on coordination mode of O<sub>2</sub> is shown for the sake of simplicity and does not necessarily reflect the actual mode in the optimized structures (see text for details).

## Results and Discussion

### Validation of the Structural Models

Superpositions of the substrate-free 6C iron species **1** and substrate-bound 5C iron species **2** with the corresponding crystal structures are shown in Figures 4 and S1 of the SI. We calculated the root mean square deviation (RMSD) between optimized structures of our fully relaxed and constrained models (see also Figure S2 in the Supporting Information). The constrained model closely resembles the crystal structure with RMSD values of 0.65 Å and 3.26 Å for **1** and **2** of the unconstrained model, respectively. Overall, we find that structure optimizations preserve the overall active site structure of NDO. The higher RMSD for **2** is due to additional degrees of

freedom for the substrate in the fully relaxed model. Despite the lack of structural constraints in this model, the substrate remains in close proximity of the active site with a distance of 4.5 Å between the iron atom and the closest-lying carbon atom of naphthalene in agreement with the crystal structure for which this distance is 4.3 Å (Figure 4). This distance increases slightly to 4.6 Å in the constrained model. In the optimized structure of compound **1**, the interatomic distances between the iron site and the oxygen atom of the axially and equatorially bound water molecules are in the range of 2.2–2.4 Å for both structure model classes and for both DFT functionals, respectively (Table 1). With the sum of covalent radii being 2.2 Å, we consider both water ligands being covalently bound to the metal center. Ohta et al.<sup>[41]</sup> observed an elongation of the axial Fe–O<sub>water</sub> bond as soon as the Rieske cluster was reduced and

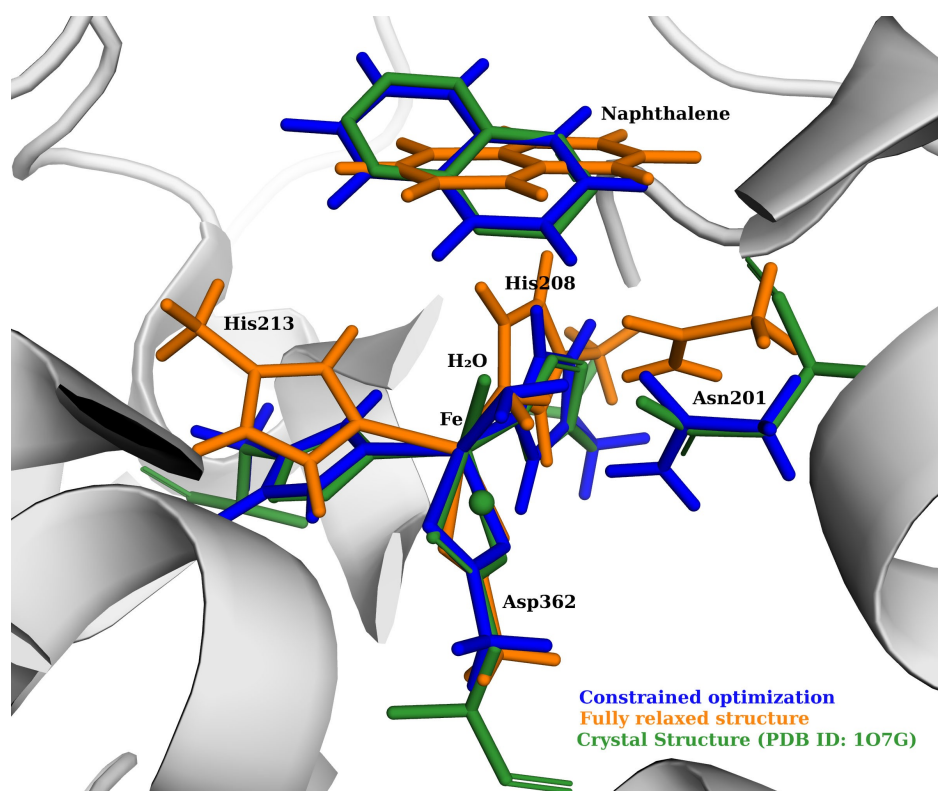


**Figure 4.** Superposition of the crystal structure (PDB-ID: 1O7G) with the PBE-D3/def2-TZVP optimized structures of the constrained (blue) and fully relaxed (orange) models of compound **2**. The structures were aligned at the iron center and the terminal carbon atoms of Asn<sub>201</sub> and His<sub>213</sub>. The crystal structure depicts only one solvent molecule that is bound to the metal center. The second-closest solvent molecule is visualized by a green sphere.

**Table 1.** Selected PBE-D3/def2-TZVP and PBE0-D3/def2-TZVP (in parentheses) inter-atomic distances in Å of the metal center to the oxygen atom of the water ligands and ligating H<sub>2</sub>O molecules in compounds **1**, **1'**, and to one carbon atom of naphthalene in compound **2**, respectively, in Å. The subscripts ax and eq refer to the axially and the equatorially coordinated water ligand, respectively, where the latter one establishes a hydrogen bond to the second-sphere Asn<sub>201</sub>. Subscript NPY denotes naphthalene.

	<b>1</b> Fe–O <sub>(H<sub>2</sub>O–ax)</sub>	Fe–O <sub>(H<sub>2</sub>O–eq)</sub>	<b>1'</b> Fe–O <sub>(H<sub>2</sub>O–ax)</sub>	Fe–O <sub>(H<sub>2</sub>O–eq)</sub>	<b>2</b> Fe–C <sub>(NPY)</sub>
fully relaxed	2.4 (2.2)	2.2 (2.4)	3.5 (3.5)	2.2 (2.2)	4.5 (4.5)
constrained	2.3 (2.3)	2.3 (2.2)	3.2 (3.1)	2.3 (2.3)	4.6 (4.5)

hence was ready to transfer an electron to the non-heme Fe center. After electron transfer, the resulting species corresponds to intermediate **1'** in our notation. We find that the Fe–O<sub>water</sub> bond elongates to 3.2 Å and 3.5 Å in the constrained and fully relaxed model in **1'**, respectively, upon addition of an electron (Table 1). The mean absolute deviation (MAD) in calculated interatomic distances for **1**, **1'** and **2** between the two density functionals PBE and PBE0 is only 0.07 Å, where PBE bond lengths are slightly shorter compared to PBE0.

#### Six-to-Five Coordinate Conversion and Substrate Binding

The release of a solvent ligand and the ensuing 6C to 5C reduction in coordination number at the non-heme Fe<sup>II</sup> center appears to be initiated by the presence of the substrate in the active site pocket.<sup>[9,20–22,24,30,40–42]</sup> However, crystallographic and

spectroscopic data do not provide direct evidence for the correlation of these molecular events. Here, we split the 6C to 5C conversion into separate steps of substrate binding and water abstraction as shown in Figure 5, which shows a subset of oxidized species in the reaction network in Figure 3. In agreement with previous work,<sup>[90]</sup> we find that the non-heme Fe<sup>II</sup> center in the high-spin quintet state is the most stable spin state for all structures displayed in Figure 5 (see data in Figure S3 in the SI). This observation is in agreement with previous work from Bassan et al.<sup>[90]</sup> and holds true for both classes of structures. As introduced in Figure 3, we evaluated two processes for the abstraction of the axial water ligand: One in which the abstraction of H<sub>2</sub>O is guided by the Asn<sub>201</sub> residue that keeps the ligand in the second coordination sphere through hydrogen bonding (reaction **1**→**2**) vs. complete abstraction of H<sub>2</sub>O yielding species **3**.

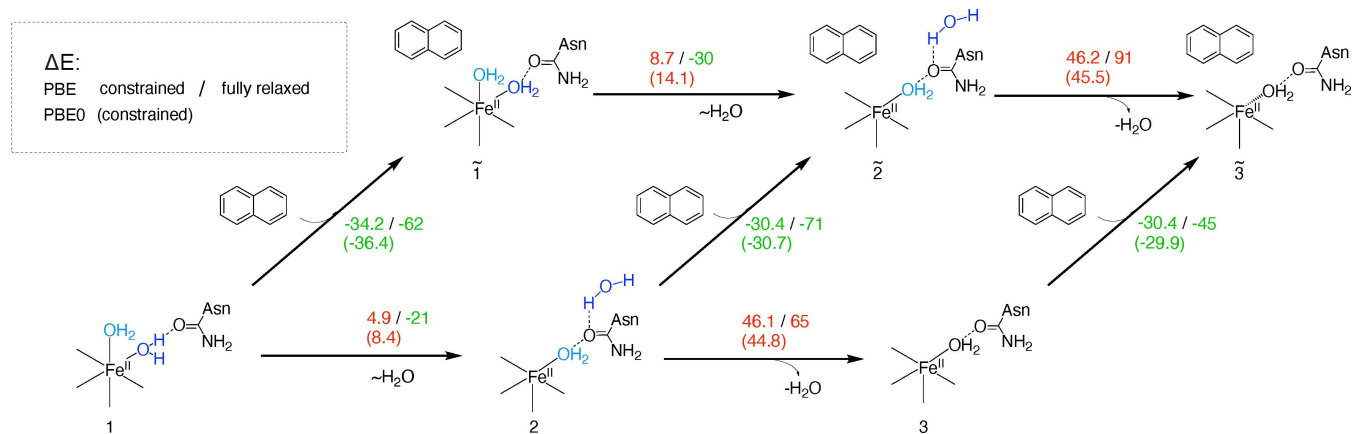


**Figure 5.** PBE-D3/def2-TZVP (PBE0-D3/def2-TZVP in parentheses) electronic energy differences of the reaction network associated with the 6C to 5C conversion at the non-heme Fe<sup>II</sup> center in NDO. The slash notation refers to the two model classes: constrained/fully relaxed. All energies are given in kJ mol<sup>-1</sup>. All horizontal arrows refer to solvent reorientation or dissociation and diagonal arrows are associated with substrate binding. Red and green numbers indicate an overall endothermic and exothermic reactions, respectively.

### Water Reorientation versus Water Abstraction

We examined the dissociation of the two water molecules (colored in blue and turquoise in Figure 5) coordinated equatorially and axially in a distorted octahedral environment of species 1. Regardless of which ligand dissociates, the remaining H<sub>2</sub>O ligand occupies the equatorial position, (consequently, the ligands can be considered interchangeable) which is stabilized by a hydrogen bond to the Asn<sub>201</sub> residue. This step renders the axial coordination position vacant and directed towards the substrate (Figure 5). This finding is supported by the analysis of substrate binding in NDO in the presence of nitric oxide as non-reactive O<sub>2</sub> surrogate at the non-heme Fe center, indicating that O<sub>2</sub> and one solvent molecule bind at the active site.<sup>[58]</sup> Our finding of water dissociation that is assisted by hydrogen bonding to Asn<sub>201</sub> stands in contrast to the generally accepted mechanistic hypothesis for NDO activation. Compared to full abstraction, hydrogen bond enhanced dissociation is almost thermoneutral with reaction energies of 4.9 kJ mol<sup>-1</sup> without substrate and 8.7 kJ mol<sup>-1</sup> with substrate in the constraint model. The reactions are even fully exothermic by -21 and -30 kJ mol<sup>-1</sup> (without and with substrate, respectively) in the relaxed model (with PBE0, 8.4 and 14.1 in the constrained model, respectively). Hence, 2 and  $\tilde{2}$  likely bind dioxygen while formation of 3 and  $\tilde{3}$  is endothermic by more than 45 kJ mol<sup>-1</sup>. As 5C species 2 and  $\tilde{2}$  are formed in an overall exothermic reaction, 3 and  $\tilde{3}$  will not be considered in further steps. The reorientation of one first-shell water ligand towards the second shell is also supported by several different NDO crystal structures (107H and 107G,<sup>[38]</sup> 1UUW,<sup>[91]</sup> 1EG9<sup>[39]</sup>) that show one solvent molecule coordinated to the non-heme iron center at a distance of 2.1–2.3 Å and a second one in the second coordination sphere at a distance of 4.1–4.2 Å. The reaction energies in Figure 5 show that the PBE0 hybrid density functional delivers reaction energies of the water reorientation steps (1→2 and  $\tilde{1}$ → $\tilde{2}$ ) that are less than a factor of two (8.4 vs. 4.9 kJ mol<sup>-1</sup> and 14 vs. 8.7 kJ mol<sup>-1</sup>, respectively)

higher than those obtained with PBE. The reaction energies for the formation of 2 and  $\tilde{2}$  are therefore not high enough to prevent a spontaneous reaction under standard conditions. Evaluation of the activation barriers for elementary steps of reactions 1→2 and  $\tilde{1}$ → $\tilde{2}$  further show a flat energy profile with reaction barriers sufficiently low for the reaction to occur spontaneously (see also Figure S4 in the Supporting Information).

### Effect of the Substrate

We compared the upper and lower thread of the reaction mechanism in Figure 5 to assess the role of the substrate in the active site pocket on the 6C to 5C change in coordination number. Water ligand reorientation in the presence of naphthalene ( $\tilde{1}$ → $\tilde{2}$ ) is energetically equivalent to the substrate-free reaction (1→2). This finding contrasts previous hypotheses that substrate binding facilitates the release of one solvent molecule.<sup>[32,41]</sup> Substrate binding itself is exothermic by more than -30 kJ mol<sup>-1</sup> for the constrained system and -45 to -71 kJ mol<sup>-1</sup> for the fully relaxed one, depending on whether the substrate is added to species 1, 2, or 3. The substrate interaction with the active site can be ascribed to dispersive attraction as 85% of the reaction energy are recovered by summing up all pairwise dispersion interactions that include substrate atoms (Table S1 in the Supporting Information). Even though a vacant coordination site has been established at the non-heme Fe center, naphthalene remains at 4.8 Å distance and does not coordinate to the Fe atom, as it is, e.g., the case for extradiol dioxygenases, where the substrate covalently binds to the metal site. This behavior is typical for RDOs. Note also that the dispersion enhanced substrate binding in our model is an artifact because we neglect the dispersion energies that stabilize naphthalene before it approaches its binding pocket, because we consider the substrate to emerge from a dispersion-free environment (i.e., in vacuo). The data presented in

Table 1 and Figure 5 for coordination changes at the non-heme Fe site, water reorientation, and substrate binding reveal identical interpretations for the fully relaxed and constraint model classes in the two elementary steps discussed above. The subsequent discussion will therefore be based on the constrained model class.

### Dioxygen Coordination

Dioxygen coordination at the non-heme Fe<sup>II</sup> center is closely tied to the ensuing electron transfer from the Rieske cluster. Previous studies on NDO<sup>[54]</sup> and BZDO<sup>[33]</sup> suggest that O<sub>2</sub> binding is thermoneutral or even endothermic also due to entropic losses related to O<sub>2</sub> binding. Here, we now systematically evaluate energy and structural aspects with regard to the sequence of O<sub>2</sub> binding and Rieske cluster oxidation in the presence and absence of the substrate naphthalene. We also extend the relevant range of spin configurations considered by evaluating spin states from  $S=0$  up to  $S=6$ . For dioxygen-free compounds, the expected spin state range is spanned by the typical  $d$ -configuration of Fe<sup>II</sup>, Fe<sup>III</sup> or, after reduction, by the unlikely Fe<sup>I</sup> species. For species that contain an O<sub>2</sub> molecule, this range is extended by all possible combinations of ferro- and antiferromagnetic coupling of  $d$ -configurations at the Fe site with either <sup>3</sup>O<sub>2</sub> or <sup>1</sup>O<sub>2</sub>. We take the sum of covalent radii of iron and oxygen being 2.2 Å as a threshold for the covalent bond assignment.<sup>[92,93]</sup>

### Dioxygen Coordination Prior to Electron Transfer from the Rieske Cluster

The iron-oxygen species for all oxidized species containing O<sub>2</sub>, namely  $\tilde{1}^{O_2}$ ,  $\tilde{2}^{O_2}$ ,  $1^{O_2}$ , and  $2^{O_2}$  may be either of ferrous-oxo- (Fe<sup>II</sup>-O<sub>2</sub>), ferric-superoxo-(Fe<sup>III</sup>-O<sub>2</sub><sup>-</sup>), or Fe<sup>IV</sup>-peroxo-(Fe<sup>IV</sup>-O<sub>2</sub><sup>2-</sup>)-type with a high-spin iron center stabilized by the 2-His-1-carboxylate facial triad.<sup>[90,94,95]</sup>

For the 6C structures  $1^{O_2}$  and  $\tilde{1}^{O_2}$  without and with substrate, respectively, we found the high-spin septet state to be the ground state for both density functionals in agreement with experimental observations.<sup>[41]</sup> For the 5C structures  $2^{O_2}$  and  $\tilde{2}^{O_2}$ , however, we encounter the known limitations of pure density functionals such as the PBE density functional with respect to characterizing open-shell species<sup>[96–98]</sup> (Table S4 in the Supporting Information). PBE-optimized structures adopt a singlet state with no unpaired electrons at the non-heme Fe<sup>II</sup> center and O<sub>2</sub>, whereas PBE0-optimized structures converge towards the high-spin septet states as expected<sup>[96–98]</sup> (Table S5 in the Supporting Information). The singlet ( $S=0$ ) ground state for PBE-optimized structures of  $2^{O_2}$  and  $\tilde{2}^{O_2}$  would correspond to a change of total spin, because unbound O<sub>2</sub> adopts a triplet spin state in its ground state and the resting non-heme Fe site is a ferrous site in a quintet state (see above). Although high-spin states are systematically favored by the admixture of exact exchange to the DFT functional,<sup>[96,98]</sup> which is zero even with PBE, we find small energy gaps between the low-spin singlet

state and the high-spin septet state for PBE with 7.7 kJ mol<sup>-1</sup> for  $\tilde{2}^{O_2}$  and 29.5 kJ mol<sup>-1</sup> for  $2^{O_2}$ . Conversely for PBE0, the septet state is stabilized by -156.3 kJ mol<sup>-1</sup> for  $\tilde{2}^{O_2}$ , but only by -1.2 kJ mol<sup>-1</sup> for  $2^{O_2}$ . In view of the recurring high-spin motif within RDOs stabilized by the facial triad, we focus our subsequent discussion on data obtained for PBE0-optimized structures that point towards more reasonable ground state spin states. The complete set of results is compiled in section S4 of the Supporting Information. CCSD(T)/def2-TZVP single-point calculations were carried for on all ground state structures obtained from PBE0 structure optimizations. For a detailed discussion of spin configuration, spin populations, Fe–O and O–O interatomic distances and spin state energetics of the discussed compounds, we refer to Tables S5 and S6 in the Supporting Information.

Figure 6 summarizes our findings of dioxygen coordination at 6C and C non-heme Fe<sup>II</sup> species. Electronic energy differences for the displayed reactions ( $\tilde{1}^{O_2} \rightarrow \tilde{1}^{O_2}/\tilde{2}^{O_2}$  and  $1/2 \rightarrow 1^{O_2}/2^{O_2}$ ) are almost thermoneutral throughout (within a range of -11.7 to -15.4 kJ mol<sup>-1</sup>). All trends of DFT reaction energies are reproduced in the coupled cluster calculations and they slightly underestimate PBE0 reaction energies by 2–7 kJ mol<sup>-1</sup> (numbers in parentheses in Figure 6). Both 6C non-heme Fe<sup>II</sup> sites  $1^{O_2}$  and  $\tilde{1}^{O_2}$  clearly do not exhibit activated O<sub>2</sub> species: Fe–O distances displayed in Figure 6 for  $1^{O_2}$  and  $\tilde{1}^{O_2}$  are 4.6 Å and 4.9 Å, respectively, indicating the complete lack of bonding between O<sub>2</sub> and the Fe site. Instead, O<sub>2</sub> remains in the vicinity of the axial solvent ligand (Figure 6). By contrast, the 5C species present an open unsaturated site at the octahedral polyhedron capable of coordinating O<sub>2</sub>. Still, we find that in the absence of the substrate naphthalene in species  $2^{O_2}$ , O<sub>2</sub> remains at a distance of 3.5 Å from the non-heme Fe<sup>II</sup> center. In this case, the Wiberg bond order of zero highlights the lack of an Fe–O bond. The septet-triplet spin splittings are 117.0 and 72.6 kJ mol<sup>-1</sup> for  $\tilde{2}^{O_2}$  and  $2^{O_2}$  (Table S5 in the Supporting Information) which implies that antiferromagnetic coupling between the non-heme Fe<sup>II</sup> site and O<sub>2</sub> is unlikely to occur. Only in the presence of naphthalene ( $\tilde{2}^{O_2}$ ) we observed Fe–O and O–O bond lengths of 2.2 Å and 1.3 Å, respectively, in good agreement with the sum of covalent radii. In  $\tilde{2}^{O_2}$ , the spin excess population is 4.08 (4.64) on Fe and 1.53 (1.15) on O<sub>2</sub> for PBE0 (Coupled cluster) and the bond orders for Fe and each of the two oxygen atoms are 0.47 (0.37) and 0.42 (0.29), respectively. These PBE0 data point towards a  $d^6$ -Fe<sup>II</sup>-O<sub>2</sub> species in  $\tilde{2}^{O_2}$  for PBE0-optimized structures, where iron is in the ferrous state incapable of reducing O<sub>2</sub> to a superoxide.<sup>[44]</sup> Coupled cluster data, however, indicate a  $d^5$ -Fe<sup>III</sup>-O<sub>2</sub><sup>-</sup> species which is considered one of the reactive Fe-oxygen species of RDOs.<sup>[32,33]</sup> From the energy point of view, however, the thermoneutrality of O<sub>2</sub> coordination with a coordination energy of only -15.4 (-7.1) kJ mol<sup>-1</sup> ( $\tilde{2} \rightarrow \tilde{2}^{O_2}$ ) is far too small to consider the dioxygen species activated. Our data consistently show that prior to Rieske cluster oxidation, dioxygen does not bind covalently to the oxidized non-heme Fe<sup>II</sup> center, reflected in the thermoneutrality of O<sub>2</sub> coordination to both 6C and 5C species. We conclude therefore that O<sub>2</sub> remains unbound in all species.



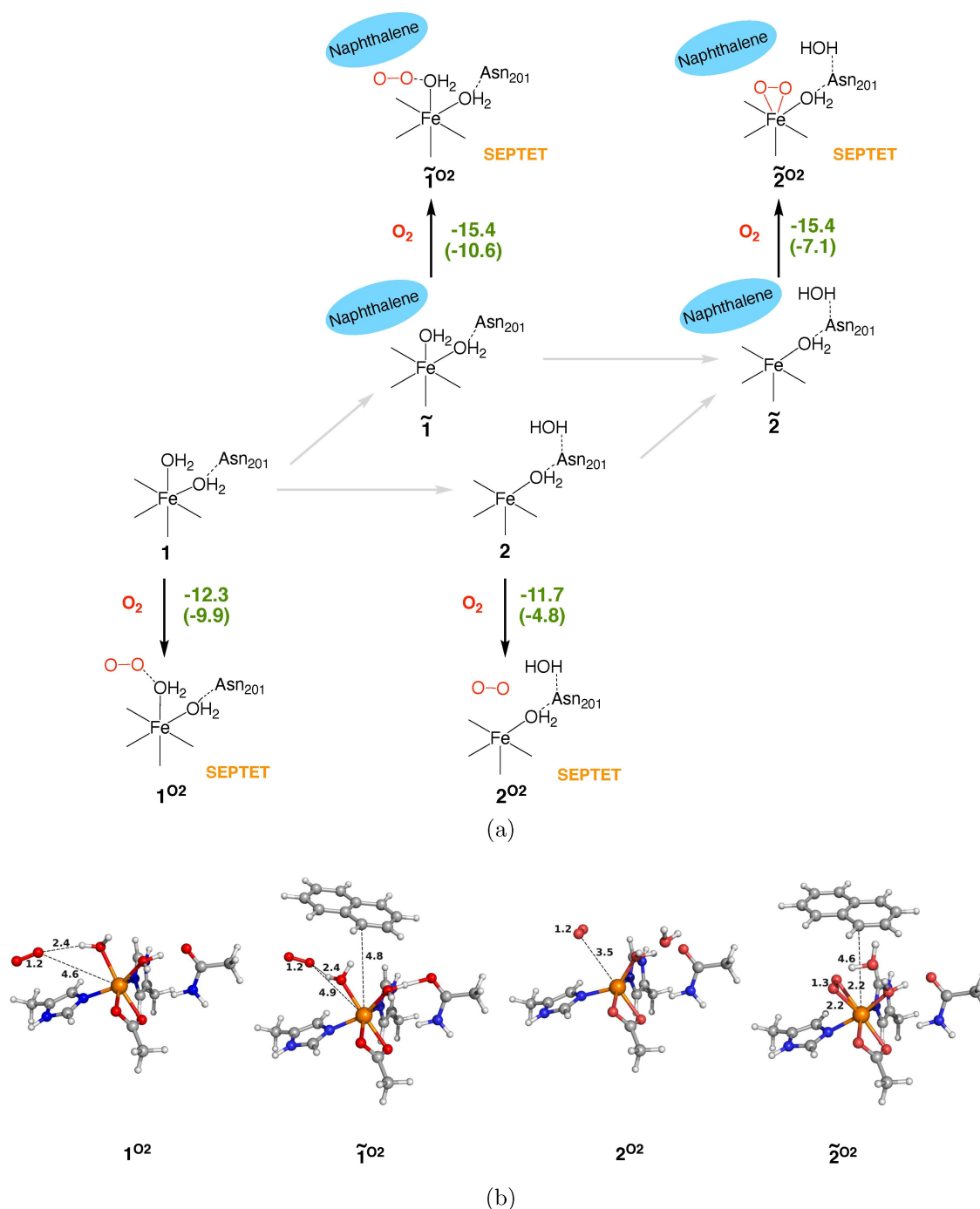


**Figure 6.** Reaction energies (a) and selected optimized structures (b) of the reactions associated with  $O_2$  coordination to the non-heme  $Fe^{II}$  center prior to electron transfer from the proximate Rieske cluster. Energies for PBE0-D3/def2-TZVP and DLPNO-CCSD(T)/def2-TZVP (the latter shown in parentheses) are given in  $\text{kJ mol}^{-1}$ . All bond lengths are given in  $\text{\AA}$ .

Moreover, naphthalene appears to have no effect on the  $O_2$  coordination to the oxidized sites.

#### Dioxygen coordination after electron transfer from the Rieske cluster

The effect of transferring an electron from the Rieske cluster to the non-heme Fe center on coordination of dioxygen was evaluated by adding one electron to all optimized structures followed by structure reoptimization for doublet, quartet, and sextet spin states. These species are denoted by a superscript *r*.

Relative energies, spin configurations, and bond length are given in Tables S7 and S8 in the Supporting Information. Data for relative PBE0 and coupled cluster reaction energies are shown in Figure 7.

We find sextet spin states as ground states for all O<sub>2</sub>-containing structures. However, the sextet-quartet spin splittings are rather small (19.0 and 28.5 kJ mol<sup>-1</sup> for  $\tilde{2}^{r-O_2}$  and  $2^{r-O_2}$  and only 2.5 and 0.9 kJ mol<sup>-1</sup> for  $\tilde{1}^{r-O_2}$  and  $1^{r-O_2}$ , Table S8 in the SI), which is indication of potential thermal spin cross-over. We found no O<sub>2</sub> coordination to the 6C sites  $1^{r-O_2}$  and  $\tilde{1}^{r-O_2}$  (Figure 7). Instead, a proton is abstracted from the axial solvent molecule. Coordination energies for dioxygen addition are, contrary to the oxidized species, highly exothermic by at least -180 kJ mol<sup>-1</sup>. PBE0 data show no effect of the substrate whereas differences are substantial for coupled cluster data (-189.9 kJ mol<sup>-1</sup> vs. -264.7 and -273.3). The intermediate  $\tilde{1}^r$  seems to be stabilized by more than 60 kJ mol<sup>-1</sup> with respect to  $\tilde{2}^r$  and 33.5 kJ mol<sup>-1</sup> relative to  $1^r$  (upon correction for the substrate coordination energy). This difference will be discussed in terms of stabilization of  $\tilde{1}^r$  due to the presence of the substrate below. At the reduced 5C sites  $2^{r-O_2}$  and  $\tilde{2}^{r-O_2}$ , O<sub>2</sub> binds with -207.5 and -199.3 kJ mol<sup>-1</sup>, respectively, according to the PBE0 results (Figure 7). Coupled cluster reaction energies for reactions  $2^r/\tilde{2}^r \rightarrow 2^{r-O_2}/\tilde{2}^{r-O_2}$  are more exothermic (up to

-276 kJ mol<sup>-1</sup>) and do not reveal any effect of the substrate. In PBE0 optimized structures, the Fe-O bond distance converges to 2.0 and 2.1 Å for  $2^{r-O_2}$  and  $\tilde{2}^{r-O_2}$ , respectively (insets in Figure 7). In the absence of the substrate (i.e., in  $2^{r-O_2}$ ), the Fe-O bond has end-on character suggesting an [Fe<sup>II</sup>- $\eta^1$ -O<sub>2</sub><sup>-</sup>]. Conversely, in  $\tilde{2}^{r-O_2}$ , the Fe-O bond is side-on corresponding to an [Fe<sup>II</sup>- $\eta^2$ -O<sub>2</sub><sup>-</sup>]. The O-O bond length was found to be 1.3 Å in both 5C species (Table S8 in the Supporting Information), in good agreement with low-temperature crystal structure data available of NDO.<sup>[38]</sup> The bond orders of the iron atom and the two O atoms were 0.39 and 0.07 for  $2^{r-O_2}$  and 0.44 and 0.46 for  $\tilde{2}^{r-O_2}$ , indicating the formation of one covalent bond ( $\eta^1$ ) in the absence of naphthalene vs. two covalent bonds ( $\eta^2$ ) in its presence. Spin excess populations for Fe of 3.7 to 3.9 (Table 2) suggest that the non-heme Fe center remains in the ferrous oxidation state, whereas the O<sub>2</sub> molecule is reduced to a superoxide species. This interpretation is reflected in  $\alpha$ -spin excess populations for PBE0 and coupled cluster data (in parentheses) for  $2^{r-O_2}$  and  $\tilde{2}^{r-O_2}$  of 1.00 (1.03) and 1.15 (1.09), respectively. The corresponding partial charges on O-O in the absence and presence of naphthalene amount to -0.47 (-0.51) and -0.32 (-0.38) elementary charges in total on both oxygen atoms (Table 2). The assignment of an Fe<sup>II</sup>-O<sub>2</sub><sup>-</sup> species as the activated form of O<sub>2</sub> is consistent with the other work for

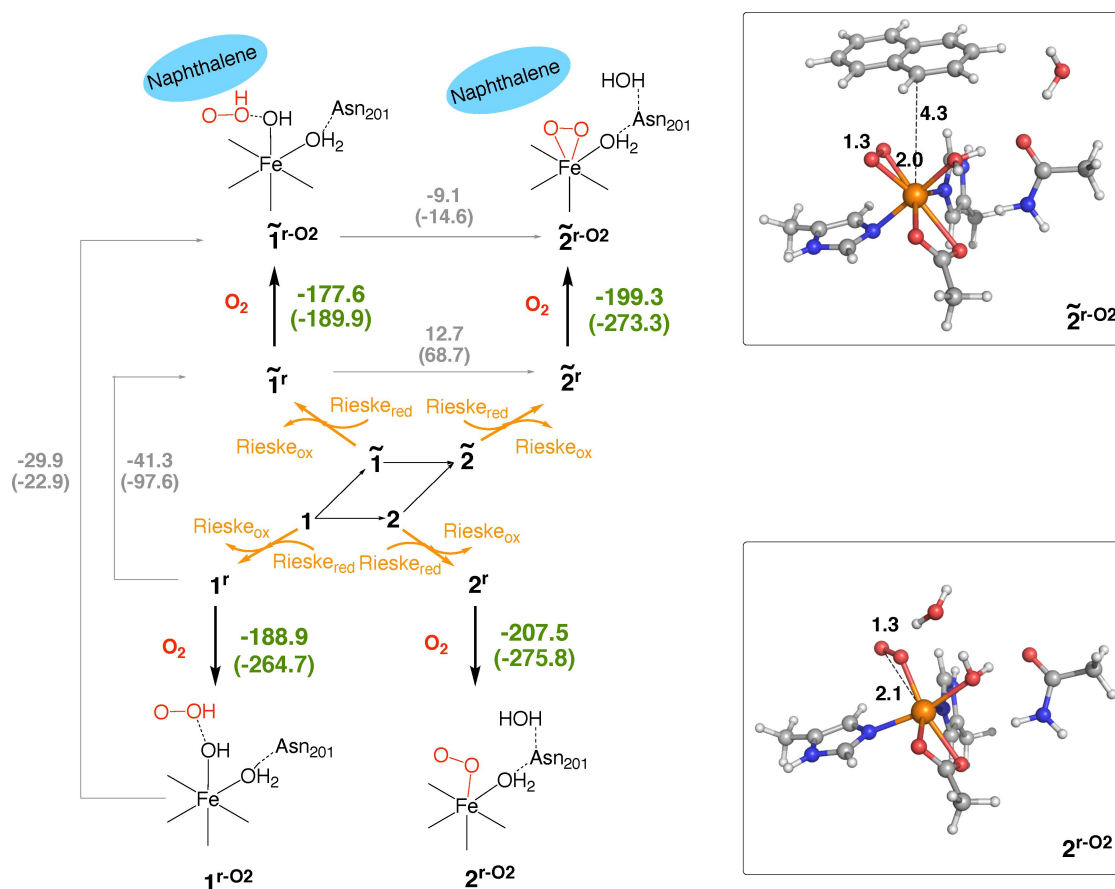


**Figure 7.** Reaction energies and selected optimized structures relevant for O<sub>2</sub> coordination to the non-heme Fe center in the presence of an additional electron (i.e., after one-electron reduction). Data for PBE0-D3/def2-TZVP and coupled cluster (in parentheses) in kJ mol<sup>-1</sup>. Orange colored arrows represent the electron transfer from the reduced Rieske cluster (R<sub>red</sub>).

		$2^{02}$	$\tilde{2}^{02}$	$2^{r-02}$	$\tilde{2}^{r-02}$
Ground state multiplicity		Septet	Septet	Sextet	Sextet
$\langle S_{z,Fe} \rangle$	Fe	3.75 (3.89)	4.08 (4.64)	3.76 (3.89)	3.69 (3.83)
	O–O	2.00 (2.00)	1.53 (1.15)	1.00 (1.03)	1.15 (1.09)
local charge on O–O		–0.00 (0.03)	–0.03 (–0.39)	–0.47 (–0.51)	–0.32 (–0.38)
bond lengths [Å]	Fe–O	3.7	2.2	2.1	2.0
	O–O	1.2	1.3	1.3	1.3
type of Fe–O bond activated oxygen species		-- <b>none</b>	side-on <b>none</b>	end-on <b>superoxo</b>	side-on <b>superoxo</b>

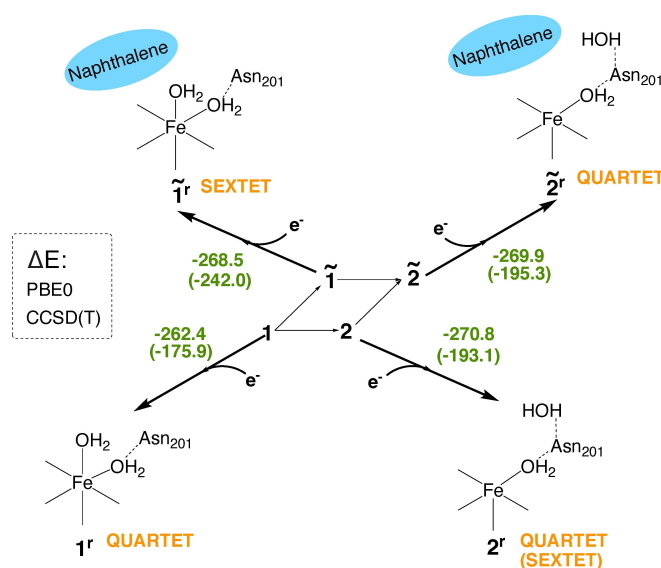
RDOs<sup>[32,33]</sup> although an Fe-peroxo species has been implied in earlier studies with NDO.<sup>[38,99]</sup>

Table 2 summarizes the structural and electronic evidence for the 5C species prior and after electron transfer from the Rieske cluster ( $2^{02}/\tilde{2}^{02}$  vs.  $2^{r-02}/\tilde{2}^{r-02}$ ). The active site remains in the non-heme Fe<sup>II</sup> state in all species. Combined data for O–O spin excess populations and local charges as well as O–O bond length and the corresponding reaction energies from Figure 6 illustrate that O<sub>2</sub> does not bind to the active site in the absence of the extra electron despite short Fe–O internuclear distances in  $\tilde{2}^{02}$ . Conversely, O–O spin excess populations close to 1.00 and negative O–O charges together with typical O–O bond length point towards O<sub>2</sub> activation as Fe-superoxide species after Rieske cluster oxidation. While this process is very exothermic, it does not provide any indication for the effect of the substrate on the active site.

### Role of Distant Substrate During Electron Transfer

Our data summarized in Figures 5, 6, and 7 show that the presence of naphthalene in the active site neither triggers the 6C to 5C conversion of the non-heme Fe<sup>II</sup> center nor does it exert any notable effect on O<sub>2</sub> coordination at the 5C site. We therefore evaluated the effect of substrate presence onto the electron transfer from the Rieske cluster given that previous calculations for NDO<sup>[44]</sup> characterized this process exclusively in the absence of naphthalene. Under such conditions, the electron affinity of the non-heme Fe<sup>II</sup> only exceeded the one of the Rieske cluster if O<sub>2</sub> is bound. This approach might have been somewhat simplistic and did not account for early experimental evidence showing the lack of O<sub>2</sub> consumption by NDO in the absence of the substrate.<sup>[100]</sup>

Here, we evaluate the electron affinities of the 6C and 5C species in the absence and presence of naphthalene (Figure 8) and account for electronic relaxation processes that were found relevant for electron transfers in such systems<sup>[101–103]</sup> (see Table S11 in the Supporting Information). Adiabatic electron affinities of  $1$ ,  $2$ ,  $\tilde{1}$  and  $\tilde{2}$  (reduced species carry superscript r) of



**Figure 8.** PBE0-D3/def2-TZVP energies of reactions associated with the one-electron reduction in naphthalene 1,2-dioxygenase. All energies are in kJ mol<sup>−1</sup>, DLPNO–CCSD(T)/def2-TZVP results are given in parentheses.

–262.4 to –270.8 kJ mol<sup>−1</sup> are more exothermic compared to the adiabatic ionization energy of the Rieske cluster that we calculated to be 175.3 kJ mol<sup>−1</sup> (all obtained with PBE0-D3/def2-TZVP). This points toward an irreversible electron transfer, which was also recently reported for the O<sub>2</sub> activation by other RDOs (i.e., BZDO<sup>[33]</sup>).

Whilst DFT results show no difference in electron affinities with and without the substrate, the coupled cluster results put this into a slightly different perspective: The electron affinity of  $\tilde{1}^r$  is more than 60 kJ mol<sup>−1</sup> more negative than that of all other species. The increased electron affinity of  $\tilde{1}^r$  with respect to the other species depicted in Figure 8 results in a stabilization of  $\tilde{1}^r$ . As a result, the O<sub>2</sub> coordination energy to species  $\tilde{1}^r$  is decreased by almost 80 kJ mol<sup>−1</sup> (for CCSD(T)) compared to the respective 5C reaction  $\tilde{2}^r \rightarrow \tilde{2}^{r-02}$  (see also Figure 7 and discussion in previous sections).

We calculated the vertical and adiabatic electron affinity of naphthalene to be slightly endothermic ( $41.8 \text{ kJ mol}^{-1}$  and  $29.1 \text{ kJ mol}^{-1}$  with PBE0/def2-TZVP). Hence, the electron affinity of naphthalene cannot be the driving force for the process. Instead, we found a highly exothermic binding of the naphthalene anion to the metal fragment **1**, i.e.,  $\text{NPY}^{\text{anion}} + \mathbf{1} \rightarrow \tilde{\mathbf{1}}^{\text{r}}$  ( $-332.7 \text{ kJ mol}^{-1}$  with PBE0, which is in excellent agreement with the  $-326.9 \text{ kJ mol}^{-1}$  obtained with CCSD(T)), which produces a thermodynamic sink for the electron transfer. From comparison with the Hartree-Fock result for the naphthalene anion binding energy of  $-262.6 \text{ kJ mol}^{-1}$ , we may estimate a contribution of  $64.3 \text{ kJ mol}^{-1}$  of dispersion interactions to naphthalene anion binding at the metal site (if we assume that all dynamical correlation energy can be assigned to attractive dispersive forces; for comparison, the D3 dispersion contribution is of the same magnitude and amounts to  $-34.7 \text{ kJ mol}^{-1}$ ).

The evaluation of spin states as well as spin excess populations at the non-heme Fe center and naphthalene across different computational methods discussed below suggests that the notably larger electron affinity of  $\tilde{\mathbf{1}}$  is likely due to contributions of the substrate to the electron transfer from the Rieske cluster and formation of  $\tilde{\mathbf{1}}^{\text{r}}$ .  $\tilde{\mathbf{1}}^{\text{r}}$  exhibits an unexpected sextet spin state as its ground state for both PBE0 and coupled cluster data (see Tables 3 and S12), whereas species **1**<sup>r</sup> and  $\tilde{\mathbf{2}}^{\text{r}}$  preferably adopt the quartet spin states. For **2**<sup>r</sup>, the PBE0 data suggest a quartet spin state, whereas CC calculations point towards the high-spin sextet spin state. In the absence of naphthalene, where the additional electron can be localized solely at the transition metal site, a quartet spin state shows  $\alpha$ -spin excess population of about 3  $\alpha$ -electrons (i.e., 2.99 for **1**<sup>r</sup> and 3.14 for **2**<sup>r</sup>, see Table 3) which is the unlikely  $d^7\text{-Fe}^{\text{I}}$  species. In  $\tilde{\mathbf{1}}^{\text{r}}$ , by contrast, the non-heme Fe remains in the ferrous oxidation state with a spin excess population of 3.76  $\alpha$ -electrons and the reducing electron is transferred to the substrate, which adopts a doublet spin state with an overall spin excess population of 0.96 and a partial charge of  $-0.88$  elementary charges (see Table 3). Hence, the incoming electron is localized at naphthalene only. This process avoids intermediate formation of the unstable  $\text{Fe}^{\text{I}}$  species. Localization of the additional electron on the substrate exclusively stabilized the 6C species  $\tilde{\mathbf{1}}^{\text{r}}$  whereas no such effect was observed in the 5C species  $\tilde{\mathbf{2}}^{\text{r}}$  (spin excess population of 0.01, Table 3). Given that these two species only differ with regard to axially coordinated  $\text{H}_2\text{O}$  ligand at  $\tilde{\mathbf{1}}^{\text{r}}$ , we hypothesize that the transfer of the Rieske electron to the substrate is mediated by this ligand. An RMSD of  $1.25 \text{ \AA}$  between  $\tilde{\mathbf{1}}$  and optimized  $\tilde{\mathbf{1}}^{\text{r}}$  reflects a considerable reorientation of the substrate towards the axial  $\text{H}_2\text{O}$  molecule in

$\tilde{\mathbf{1}}^{\text{r}}$  as depicted in Figure 9. As a consequence, the distance between the axial solvent molecule and the closest naphthalene-carbon atom decreases from  $3.6$  and  $2.1 \text{ \AA}$  in  $\tilde{\mathbf{1}}$  to  $1.9$  and  $2.5 \text{ \AA}$  in  $\tilde{\mathbf{1}}^{\text{r}}$ , allowing for a potentially allosteric control of the metal-to-substrate charge transfer via the  $\text{H}_2\text{O}$  ligand. Such an intermediate localization of negative charge at the substrate is, in a qualitative picture, corroborated by the highest occupied (HOMO) and lowest unoccupied molecular orbital (LUMO) of  $\tilde{\mathbf{1}}^{\text{r}}$ : Figure S8 in the Supporting Information shows that the HOMO of  $\tilde{\mathbf{1}}^{\text{r}}$  exhibits strong metal- $d$ -character and only very moderate naphthalene character, whereas the LUMO is almost fully localized on the substrate. Qualitative evaluation of the wave function obtained in CASSCF calculations (for a detailed Methodology, we refer to the Supporting Information, section S8) show that all structures that exclude the substrate, i.e. **1** and **2** exhibit no multireference character. For  $\tilde{\mathbf{1}}$  and  $\tilde{\mathbf{2}}$ , the orbital entanglement pattern is more complex, not limiting the involved orbitals to the Fe- $d$ -orbital set only, but also including the  $\pi$ -orbitals of naphthalene. For  $\tilde{\mathbf{1}}^{\text{r}}$ , we obtained strong localization of singly occupied orbitals on the substrate, converging to a total charge of  $-0.86$  elementary charges on the substrate. Full-valence DMRG-CASSCF calculations on relevant structures using the autoCAS workflow developed in our group<sup>[79,81–83,104]</sup> support this substrate-assisted electron transfer for  $\tilde{\mathbf{1}}^{\text{r}}$  (see Figures S11–S16 and in particular Figures S15 and S16 and discussion in section S8 in the Supporting Information). We find that the electron transfer to the substrate persists for non-relaxed  $\tilde{\mathbf{1}}^{\text{r}}$ . The phenomenon is apparent not only in the sextet spin state, but also in the quartet spin state, with both states being energetically close by  $3.4 \text{ kJ mol}^{-1}$  (Table S12). These results imply that electronic relaxation following the electron transfer is not critical.

Hence, the role of the substrate in the active site pocket may be to first accommodate the electron transferred from the Rieske cluster to the non-heme Fe. We find this contribution of the substrate only prior to  $\text{O}_2$  coordination and before the 5C-to-6C change associated with solvent reorientation. No spin excess populations in the ground state were found on the

**Table 3.** Spin excess populations for PBE0-D3/def2-TZVP and DLPNO-CCSD(T)/def2-TZVP calculations (in parentheses) at the non-heme Fe center and naphthalene on reduced species in the absence and presence of the substrate.

	(2S+1)	$\langle S_{z,\text{Fe}} \rangle$	$\langle S_{z,\text{Naphth.}} \rangle$
<b>1</b> <sup>r</sup>	4	2.99 (2.95)	–
<b>2</b> <sup>r</sup>	4	3.14 (3.88)	–
$\tilde{\mathbf{1}}^{\text{r}}$	6	3.76 (3.88)	0.96 (0.97)
$\tilde{\mathbf{2}}^{\text{r}}$	4	3.01 (2.95)	0.01 (0.00)

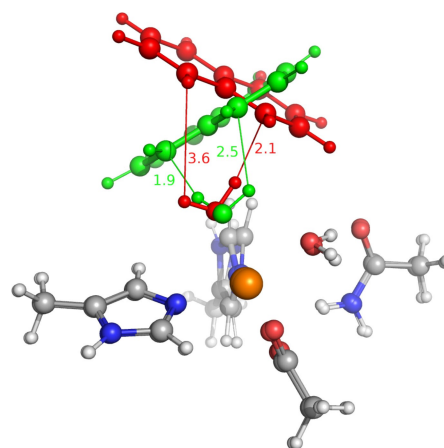


**Figure 9.** Overlay of species  $\tilde{\mathbf{1}}$  and  $\tilde{\mathbf{1}}^{\text{r}}$ . The substrate and the axial  $\text{H}_2\text{O}$  ligand are depicted in red for  $\tilde{\mathbf{1}}$  and in green for  $\tilde{\mathbf{1}}^{\text{r}}$ .

substrate in any other species containing the electron from the Rieske cluster (i.e.,  $\tilde{1}^{r-O_2}$ ,  $\tilde{2}^r$ , or  $\tilde{2}^{r-O_2}$ , see Tables S8 and S12 in the Supporting Information). Further reaction of  $\tilde{1}^r$ , namely water reorientation including 5C-to-6C changes are generally thermoneutral (Figures 5 and 7) while the stabilization of  $\tilde{1}^r$  derived from coupled cluster calculations makes this process appear endothermic. Nevertheless, O<sub>2</sub> binding at the non-heme Fe is energetically favored (Figure 7) leading to species  $\tilde{2}^{r-O_2}$  that are capable of subsequent *cis*-dihydroxylation of naphthalene.

## Conclusions

The lack of substrate coordination at the non-heme Fe center largely prevents the rationalization of the many observations of substrate-mediated O<sub>2</sub> activation and reactivity of RDOs.<sup>[105]</sup> Our systematic theoretical investigation of the initial sequence of elementary steps in the catalytic cycle of NDO reveals contributions of naphthalene to O<sub>2</sub> activation which appear closely coupled to the electron transfer from the Rieske cluster. Reaction energies for the generation of a coordination vacancy at the non-heme Fe<sup>II</sup> center through H<sub>2</sub>O reorientation and O<sub>2</sub> binding prior to Rieske cluster oxidation are largely insensitive to the presence of the substrate and do not lead to formation of any of the known reactive Fe-oxygen species. Moreover, binding naphthalene in the proximity to the active site does not, as expected, have any effect in O<sub>2</sub> coordination. We obtain consistent evidence for a possible role of the substrate only after Rieske cluster oxidation. Whereas the electron affinity of naphthalene is basically thermoneutral and cannot be the driving force for the electron transfer, the resulting naphthalene anion binds strongly to the active-site metal fragment, which provides a thermodynamic sink. The excess electron was found to be localized on the naphthalene substrate, but may be viewed as a resonance-stabilized charge. This charge localization was observed exclusively for the 6-coordinate non-heme Fe<sup>II</sup> site and would imply an allosteric control of the substrate on RDO reactivity to happen prior to the thermoneutral H<sub>2</sub>O reorientation and the exothermic O<sub>2</sub> coordination. Note that in absence of naphthalene, oxidation of the Rieske cluster does not produce a reduced species that activates O<sub>2</sub> in an energetically favorable way. Previous studies characterized the exergonic and therefore fast electron transfer from the Rieske cluster to the non-heme Fe center, but this process was shown to occur after changes of non-heme Fe coordination as well as O<sub>2</sub> binding.<sup>[32,33,44]</sup> Substrate contributions to the modulation of RDO reactivity in early steps of the catalytic cycle are meaningful to avoid unproductive O<sub>2</sub> activation. The absence of charge localization at the substrate in the reduced 5-coordinate Fe species could imply a mechanism in which H<sub>2</sub>O reorientation and O<sub>2</sub> binding are concerted processes. Further exploration of the sequence of O<sub>2</sub> activation reactions as well as substrate hydroxylation steps on the basis of a system-focused molecular mechanics models will be key for the study of the broad substrate-mediated reactivity of RDOs. In future work, we will consider QM/MM-based evaluation of RDO-mediated oxygen-

ations on the basis of atomistic and system-focused molecular mechanics models.<sup>[106,107]</sup> Such a model will eventually allow us to consider the electron transfer kinetics in a proper way, which is key to understanding the emergence of substrate-mediated activation by seemingly spectator substrates.

## Acknowledgments

This work was supported by Swiss NSF grant 200021\_172950-1. Open access funding provided by ETH-Bereich Forschungsanstalten.

## Conflict of Interest

The authors declare no conflict of interest.

## Data Availability Statement

The data that support the findings of this study are available in the supplementary material of this article.

**Keywords:** Rieske dioxygenases · metalloenzymes · bioinorganic chemistry · density functional theory · ab initio calculations

- [1] L. Que, R. Y. Ho, *Chem. Rev.* **1996**, *96*(7), 2607–2624.
- [2] R. H. Holm, P. Kennepohl, E. I. Solomon, *Chem. Rev.* **1996**, *96*(7), 2239–2314.
- [3] A. G. Prescott, P. John, *Annu. Rev. Plant Physiol. Plant Mol. Biol.* **1996**, *47*(1), 245–271.
- [4] J. P. Klinman, *J. Biol. Inorg. Chem.* **2001**, *6*(1), 1–13.
- [5] M. Costas, M. P. Mehn, M. P. Jensen, L. Que, *Chem. Rev.* **2004**, *104*(2), 939–986.
- [6] T. D. Bugg, S. Ramaswamy, *Curr. Opin. Chem. Biol.* **2008**, *12*(2), 134–140.
- [7] T. Bugg, *Introduction to Enzyme and Coenzyme Chemistry*, Ed., Blackwell Publishing Ltd., **2004**, 1–292.
- [8] M. M. Abu-Omar, A. Loaiza, N. Hontzeas, *Chem. Rev.* **2005**, *105*(6), 2227–2252.
- [9] E. G. Kovaleva, J. D. Lipscomb, *Nat. Chem. Biol.* **2008**, *4*(3), 186–193.
- [10] G. Fuchs, M. Boll, J. Heider, *Nat. Rev. Microbiol.* **2011**, *9*(11), 803–816.
- [11] E. I. Solomon, S. Goudarzi, K. D. Sutherlin, *Biochemistry* **2016**, *55*(46), 6363–6374.
- [12] Y. Wang, J. Li, A. Liu, *J. Biol. Inorg. Chem.* **2017**, *22*(2–3), 395–405.
- [13] N. P. Dunham, F. H. Arnold, *ACS Catal.* **2020**, *10*(20), 12239–12255.
- [14] M. D. White, E. Flashman, *Curr. Opin. Chem. Biol.* **2016**, *31*, 126–135.
- [15] J. E. Baldwin, E. Abraham, *Nat. Prod. Rep.* **1988**, *5*(2), 129.
- [16] F. H. Vaillancourt, D. A. Vosburg, C. T. Walsh, *ChemBioChem* **2006**, *7*(5), 748–752.
- [17] P. Falnes, A. Klungland, I. Alseth, *Neuroscience* **2007**, *145*(4), 1222–1232.
- [18] F. H. Vaillancourt, J. T. Bolin, L. D. Eltis, *Crit. Rev. Biochem. Mol. Biol.* **2006**, *41*(4), 241–267.
- [19] S. M. Barry, G. L. Challis, *ACS Catal.* **2013**, *3*(10), 2362–2370.
- [20] C. E. Bopp, H.-P. E. Kohler, T. B. Hofstetter, *Chimia* **2020**, *74*(3), 108–114.
- [21] S. Kal, L. Que, *J. Biol. Inorg. Chem.* **2017**, *22*(2–3), 339–365.
- [22] K. D. Koehntop, J. P. Emerson, L. Que, *J. Biol. Inorg. Chem.* **2005**, *10*(2), 87–93.
- [23] P. C. Bruijninx, G. van Koten, R. J. Klein Gebbink, *Chem. Soc. Rev.* **2008**, *37*(12), 2716–2744.
- [24] E. I. Solomon, T. C. Brunold, M. I. Davis, J. N. Kemsley, S. K. Lee, N. Lehnert, F. Neese, A. J. Skulan, Y. S. Yang, J. Zhou, *Chem. Rev.* **2000**, *100*(1), 235–349.
- [25] P. F. Fitzpatrick, *Annu. Rev. Biochem.* **1999**, *68*(1), 355–381.

- [26] J. K. Capyk, I. D'Angelo, N. C. Strynadka, L. D. Eltis, *J. Biol. Chem.* **2009**, *284*(15), 9937–9946.
- [27] C. A. Joseph, M. J. Maroney, *Chem. Commun.* **2007**, (32), 3338.
- [28] G. Dong, J. Lu, W. Lai, *ACS Catal.* **2016**, *6*(6), 3796–3803.
- [29] W. A. van der Donk, C. Krebs, J. M. Bollinger, *Curr. Opin. Struct. Biol.* **2010**, *20*(6), 673–683.
- [30] E. I. Solomon, K. M. Light, L. V. Liu, M. Srncic, S. D. Wong, *Acc. Chem. Res.* **2013**, *46*(11), 2725–2739.
- [31] M. B. Neibergall, A. Stubna, Y. Mekmouche, E. Münck, J. D. Lipscomb, *Biochemistry* **2007**, *46*(27), 8004–8016.
- [32] B. S. Rivard, M. S. Rogers, D. J. Marell, M. B. Neibergall, S. Chakrabarty, C. J. Cramer, J. D. Lipscomb, *Biochemistry* **2015**, *54*(30), 4652–4664.
- [33] Y. Ashikawa, B. S. Rivard, L. H. Böttger, L. V. Liu, M. S. Rogers, M. Srncic, K. Park, Y. Yoda, S. Kitao, Y. Kobayashi, M. Saito, M. Seto, M. Hu, J. Zhao, J. D. Lipscomb, E. I. Solomon, *J. Am. Chem. Soc.* **2018**, *140*(16), 5544–5559.
- [34] S. M. Resnick, D. T. Gibson, *Appl. Environ. Microbiol.* **1996**, *62*(11), 4073–4080.
- [35] D. T. Gibson, S. M. Resnick, K. Lee, J. M. Brand, D. S. Torok, L. P. Wackett, M. J. Schocken, B. E. Haigler, *J. Bacteriol.* **1995**, *177*(10), 2615–2621.
- [36] Y. Ashikawa, Z. Fujimoto, Y. Usami, K. Inoue, H. Noguchi, H. Yamane, H. Nojiri, *BMC Struct. Biol.* **2012**, *12*(1), 15.
- [37] D. J. Ferraro, L. Gakhar, S. Ramaswamy, *Biochem. Biophys. Res. Commun.* **2005**, *338*(1), 175–190.
- [38] A. Karlsson, J. V. Parales, R. E. Parales, D. T. Gibson, H. Eklund, S. Ramaswamy, *Science* **2003**, *299*(5609), 1039–1042.
- [39] E. Carredano, A. Karlsson, B. Kauppi, D. Choudhury, R. E. Parales, J. V. Parales, K. Lee, D. T. Gibson, H. Eklund, S. Ramaswamy, *J. Mol. Biol.* **2000**, *296*(2), 701–712.
- [40] E. G. Pavel, L. J. Martins, W. R. Ellis, E. I. Solomon, *Chem. Biol.* **1994**, *1*(3), 173–183.
- [41] T. Ohta, S. Chakrabarty, J. D. Lipscomb, E. I. Solomon, *J. Am. Chem. Soc.* **2008**, *130*(5), 1601–1610.
- [42] A. Bassan, M. R. Blomberg, T. Borowski, P. E. Siegbahn, *J. Inorg. Biochem.* **2006**, *100*(4), 727–743.
- [43] B. E. Haigler, D. T. Gibson, *J. Bacteriol.* **1990**, *172*(1), 457–464.
- [44] A. Bassan, M. R. A. Blomberg, T. Borowski, P. E. M. Siegbahn, *J. Phys. Chem. B* **2004**, *108*(34), 13031–13041.
- [45] R. E. Parales, J. V. Parales, D. T. Gibson, *J. Bacteriol.* **1999**, *181*(6), 1831–1837.
- [46] Z. M. Beharry, D. M. Eby, E. D. Coulter, R. Viswanathan, E. L. Neidle, R. S. Phillips, D. M. Kurtz, *Biochemistry* **2003**, *42*(46), 13625–13636.
- [47] A. Pinto, M. Tarasev, D. P. Ballou, *Biochemistry* **2006**, *45*(30), 9032–9041.
- [48] B. M. Martins, T. Svetlitchnaia, H. Dobbek, *Structure* **2005**, *13*(5), 817–824.
- [49] J. D. Rogers, M. S. Lipscomb, *Biochemistry* **2019**, *58*(52), 5305–5319.
- [50] L. V. Liu, S. Hong, J. Cho, W. Nam, E. I. Solomon, *J. Am. Chem. Soc.* **2013**, *135*(8), 3286–3299.
- [51] M. D. Wolfe, J. V. Parales, D. T. Gibson, J. D. Lipscomb, *J. Biol. Chem.* **2001**, *276*(3), 1945–1953.
- [52] S. Chakrabarty, R. N. Austin, D. Deng, J. T. Groves, J. D. Lipscomb, *J. Am. Chem. Soc.* **2007**, *129*(12), 3514–3515.
- [53] M. R. Blomberg, T. Borowski, F. Himo, R. Z. Liao, P. E. Siegbahn, *Chem. Rev.* **2014**, *114*(7), 3601–3658.
- [54] A. Bassan, M. R. Blomberg, P. E. Siegbahn, *J. Biol. Inorg. Chem.* **2004**, *9*(4), 439–452.
- [55] K. Inoue, Y. Usami, Y. Ashikawa, H. Noguchi, T. Umeda, A. Yamagami-Ashikawa, T. Horisaki, H. Uchimura, T. Terada, S. Nakamura, K. Shimizu, H. Habe, H. Yamane, Z. Fujimoto, H. Nojiri, *Appl. Environ. Microbiol.* **2014**, *80*(12), 5305–5319.
- [56] R. Friemann, M. M. Ivkovic-Jensen, D. J. Lessner, C.-L. Yu, D. T. Gibson, R. E. Parales, H. Eklund, S. Ramaswamy, *J. Mol. Biol.* **2005**, *348*(5), 1139–1151.
- [57] T. C. Yang, M. D. Wolfe, M. B. Neibergall, Y. Mekmouche, J. D. Lipscomb, B. M. Hoffman, *J. Am. Chem. Soc.* **2003**, *125*(8), 2034–2035.
- [58] T. C. Yang, M. D. Wolfe, M. B. Neibergall, Y. Mekmouche, J. D. Lipscomb, B. M. Hoffman, *J. Am. Chem. Soc.* **2003**, *125*(23), 7056–7066.
- [59] M. Y. Pau, J. D. Lipscomb, E. I. Solomon, *Proc. Nat. Acad. Sci.* **2007**, *104*(47), 18355–18362.
- [60] M. Reiher, *Chimia* **2009**, *63*(3), 140–145.
- [61] S. G. Balasubramani, G. P. Chen, S. Coriani, M. Diedenhofen, M. S. Frank, Y. J. Franzke, F. Furche, R. Grotjahn, M. E. Harding, C. Hättig, A. Hellweg, B. Helmich-Paris, C. Holzer, U. Huniar, M. Kaupp, A. Marefat Khah, S. Karbalaei Khani, T. Müller, F. Mack, B. D. Nguyen, S. M. Parker, E. Perlt, D. Rappoport, K. Reiter, S. Roy, M. Rückert, G. Schmitz, M. Sierka, E. Tapavicza, D. P. Tew, C. Van Wüllen, V. K. Voora, F. Weigend, A. Wodyński, J. M. Yu, *J. Chem. Phys.* **2020**, *152*(18), 184107.
- [62] J. P. Perdew, K. Burke, M. Ernzerhof, *Phys. Rev. Lett.* **1996**, *77*(18), 3865–3868.
- [63] M. Ernzerhof, G. E. Scuseria, *J. Chem. Phys.* **1999**, *110*(11), 5029–5036.
- [64] C. Adamo, V. Barone, *J. Chem. Phys.* **1999**, *110*(13), 6158–6170.
- [65] A. Schäfer, C. Huber, R. Ahlrichs, *J. Chem. Phys.* **1994**, *100*(8), 5829–5835.
- [66] K. Eichkorn, O. Treutler, H. Öhm, M. Häser, R. Ahlrichs, *Chem. Phys. Lett.* **1995**, *240*(4), 283–290.
- [67] K. Eichkorn, F. Weigend, O. Treutler, R. Ahlrichs, *Theor. Chem. Acc.* **1997**, *97*(1–4), 119–124.
- [68] S. Grimme, J. Antony, S. Ehrlich, H. Krieg, *J. Chem. Phys.* **2010**, *132*(15), 154104.
- [69] S. Grimme, S. Ehrlich, L. Goerigk, *J. Comput. Chem.* **2011**, *32*(7), 1456–1465.
- [70] A. C. Vaucher, M. Reiher, *J. Chem. Theory Comput.* **2017**, *13*(3), 1219–1228.
- [71] F. Neese, *Wiley Interdiscip. Rev.: Comput. Mol. Sci.* **2012**, *2*(1), 73–78.
- [72] F. Neese, F. Wennmohs, U. Becker, C. Riplinger, *J. Chem. Phys.* **2020**, *152*(22), 224108.
- [73] C. Riplinger, F. Neese, *J. Chem. Phys.* **2013**, *138*(3), 34106.
- [74] C. Riplinger, B. Sandhoefer, A. Hansen, F. Neese, *J. Chem. Phys.* **2013**, *139*(13), 134101.
- [75] I. Fdez Galván, M. Vacher, A. Alavi, C. Angeli, F. Aquilante, J. Autschbach, J. J. Bao, S. I. Bokarev, N. A. Bogdanov, R. K. Carlson, L. F. Chibotaru, J. Creutzberg, N. Dattani, M. G. Delcey, S. S. Dong, A. Dreuw, L. Freitag, L. M. Frutos, L. Gagliardi, F. Gendron, A. Giussani, L. González, G. Grell, M. Guo, C. E. Hoyer, M. Johansson, S. Keller, S. Knecht, G. Kovačević, E. Källman, G. Li Manni, M. Lundberg, Y. Ma, S. Mai, J. P. Malhado, P. Å. Malmqvist, P. Marquetand, S. A. Mewes, J. Norell, M. Olivucci, M. Oppel, Q. M. Phung, K. Pierloot, F. Plasser, M. Reiher, A. M. Sand, I. Schapiro, P. Sharma, C. J. Stein, L. K. Sørensen, D. G. Truhlar, M. Ugandli, L. Ungur, A. Valentini, S. Vancollie, V. Velyazov, O. Weser, T. A. Wesolowski, P. O. Widmark, S. Wouters, A. Zech, J. P. Zobel, R. Lindh, *J. Chem. Theory Comput.* **2019**, *15*(11), 5925–5964.
- [76] F. Aquilante, J. Autschbach, A. Baiardi, S. Battaglia, V. A. Borin, L. F. Chibotaru, I. Conti, L. De Vico, M. Delcey, I. F. Galván, N. Ferré, L. Freitag, M. Garavelli, X. Gong, S. Knecht, E. D. Larsson, R. Lindh, M. Lundberg, P. Å. Malmqvist, A. Nenov, J. Norell, M. Odellius, M. Olivucci, T. B. Pedersen, L. Pedraza-González, Q. M. Phung, K. Pierloot, M. Reiher, I. Schapiro, J. Segarra-Martí, F. Segatta, L. Seijo, S. Sen, D. C. Sergentu, C. J. Stein, L. Ungur, M. Vacher, A. Valentini, V. Velyazov, *J. Chem. Phys.* **2020**, *152*(21), 214117.
- [77] S. Keller, M. Dolfi, M. Troyer, M. Reiher, *J. Chem. Phys.* **2015**, *143*(24), 244118.
- [78] S. Keller, M. Reiher, *J. Chem. Phys.* **2016**, *144*(13), 134101.
- [79] C. J. Stein, M. Reiher, *J. Chem. Theory Comput.* **2016**, *12*(4), 1760–1771.
- [80] C. J. Stein, V. Von Burg, M. Reiher, *J. Chem. Theory Comput.* **2016**, *12*(8), 3764–3773.
- [81] C. J. Stein, M. Reiher, *Mol. Phys.* **2017**, *115*(17–18), 2110–2119.
- [82] C. J. Stein, M. Reiher, *Chimia* **2017**, *71*(4), 170–176.
- [83] C. J. Stein, M. Reiher, *J. Comput. Chem.* **2019**, *40*(25), 2216–2226.
- [84] F. Aquilante, P. Å. Malmqvist, T. B. Pedersen, A. Ghosh, B. O. Roos, *J. Chem. Theory Comput.* **2008**, *4*(5), 694–702.
- [85] P. O. Widmark, P. Å. Malmqvist, B. O. Roos, *Theor. Chim. Acta* **1990**, *77*(5), 291–306.
- [86] P. Löwdin, *J. Chem. Phys.* **1950**, *18*(3), 365–375.
- [87] K. B. Wiberg, *Tetrahedron* **1968**, *24*(3), 1083–1096.
- [88] L. The PyMOL Molecular Graphics System, Version 2.0 Schrödinger, <https://pymol.org> (accessed November 1, 2021) — The {PyMOL} Molecular Graphics System, Version ~1.8, **2015**.
- [89] B. Kauppi, K. Lee, E. Carredano, R. E. Parales, D. T. Gibson, H. Eklund, S. Ramaswamy, *Structure* **1998**, *6*(5), 571–586.
- [90] A. Bassan, T. Borowski, P. E. M. Siegbahn, *Dalton Trans.* **2004**, (20), 3153.
- [91] A. Karlsson, J. V. Parales, R. E. Parales, D. T. Gibson, H. Eklund, S. Ramaswamy, *J. Biol. Inorg. Chem.* **2005**, *10*(5), 483–489.
- [92] B. Cordero, V. Gómez, A. E. Platero-Prats, M. Revés, J. Echeverría, E. Cremades, F. Barragán, S. Alvarez, *J. Chem. Soc. Dalton Trans.* **2008**, (21), 2832–2838.
- [93] C. R. Groom, I. J. Bruno, M. P. Lightfoot, S. C. Ward, *Acta Crystallogr. Sect. B* **2016**, *72*(2), 171–179.
- [94] E. I. Solomon, *Inorg. Chem.* **2001**, *40*(15), 3656–3669.

- [95] E. I. Solomon, A. Decker, N. Lehnert, *Proc. Nat. Acad. Sci.* **2003**, *100*(7), 3589–3594.
- [96] M. Reiher, O. Salomon, B. A. Hess, *Theor. Chem. Acc.* **2001**, *107*(1), 48–55.
- [97] M. Reiher, *Inorg. Chem.* **2002**, *41*(25), 6928–6935.
- [98] O. Salomon, M. Reiher, B. A. Hess, *J. Chem. Phys.* **2002**, *117*(10), 4729–4737.
- [99] M. D. Wolfe, J. D. Lipscomb, *J. Biol. Chem.* **2003**, *278*(2), 829–835.
- [100] K. Lee, *J. Bacteriol.* **1999**, *181*(9), 2719–2725.
- [101] P. Kennepohl, E. I. Solomon, *Inorg. Chem.* **2003**, *42*(3), 679–688.
- [102] P. Kennepohl, E. I. Solomon, *Inorg. Chem.* **2003**, *42*(3), 696–708.
- [103] P. Kennepohl, E. I. Solomon, *Inorg. Chem.* **2003**, *42*(3), 689–695.
- [104] C. J. Stein, D. A. Pantazis, V. Krewald, *J. Phys. Chem. Lett.* **2019**, *10*(21), 6762–6770.
- [105] D. E. Escalante, K. G. Aukema, L. P. Wackett, A. Aksan, *J. Chem. Inf. Model.* **2017**, *57*(3), 550–561.
- [106] C. Brunken, M. Reiher, *J. Chem. Theory Comput.* **2020**, *16*(3), 1646–1665.
- [107] C. Brunken, M. Reiher, *J. Chem. Theory Comput.* **2021**, *17*(6), 3797–3813.

---

Manuscript received: November 1, 2021

Accepted manuscript online: January 24, 2022

Version of record online: February 25, 2022